

3D-WAG: Hierarchical Wavelet-Guided Autoregressive Generation for High-Fidelity 3D Shapes

Tejaswini Medi^{1,2}

Arianna Rampini²

Pradyumna Reddy²

Pradeep Kumar Jayaraman²

Margret Keuper^{1,3}

¹University of Mannheim, Germany, ²Autodesk AI Lab, ³MPI for Informatics, ³Saarland Informatics Campus

tejaswini.medi@uni-mannheim.de

Github:<https://github.com/TejaswiniMedi/3DWAG-AR>



Figure 1. 3D-WAG overview. We propose an autoregressive approach to 3D shape generation, based on the “next-scale” prediction paradigm. *Left*: Our hierarchical, multi-scale wavelet encoding enables the efficient generation of highly detailed surfaces, outperforming prior models (e.g., UDiFF [103], in the red box), and showcasing generalization in conditional 3D generation tasks, like text-to-3D. *Right*: Unconditional generation of diverse, high-fidelity shapes, supporting varied implicit spatial representations.

Abstract

Autoregressive (AR) models have achieved remarkable success in natural language and image generation, but their application to 3D shape modeling remains largely unexplored. Unlike diffusion models, AR models enable more efficient and controllable generation with faster inference times, making them especially suitable for data-intensive domains. Traditional 3D generative models using AR approaches often rely on “next-token” predictions at the voxel or point level. While effective for certain applications, these methods can be restrictive and computationally expensive when dealing with large-scale 3D data. To tackle these challenges, we introduce 3D-WAG, an AR model for 3D implicit distance fields that can perform unconditional shape generation, class-conditioned and also text-conditioned shape generation. Our key idea is to encode shapes as multi-scale wavelet token maps and use a Transformer to predict the “next higher-resolution token map” in an autoregressive manner. By redefining 3D AR generation task as “next-scale” prediction, we reduce the computational cost of generation compared to traditional “next-

token” prediction models, while preserving essential geometric details of 3D shapes in a more structured and hierarchical manner. We evaluate 3D-WAG to showcase its benefit by quantitative and qualitative comparisons with state-of-the-art methods on widely used benchmarks. Our results show 3D-WAG achieves superior performance in key metrics like Coverage and MMD, generating high-fidelity 3D shapes that closely match the real data distribution.

1. Introduction

The advent of autoregressive (AR) large language models (LLMs) like the GPT series [1, 5, 62, 65, 66] and follow-up works [2, 3, 16, 21, 35, 76, 77, 79, 80] has revolutionized natural language processing by enabling highly sophisticated text generation, comprehension, and interactive capabilities across a wide range of applications. These models exhibit impressive generality and versatility, despite challenges like hallucinations [24]. At the core of these models is a self-supervised learning strategy that predicts the next token in a sequence: a simple yet powerful approach. Studies have highlighted the scalability and generalization ability of these AR-based LLMs, with scaling laws

[30] enabling the prediction of larger model performance from smaller ones. Their zero/few-shot learning capability [5, 66] showcases their adaptability to diverse, unseen tasks.

At the same time, works like VQGAN [91] and DALL-E [67] along with recent advancements [37, 69, 90] demonstrate the potential of AR models in image generation. More recently, AR models [42, 78, 93] have shown to outperform diffusion models on image generation tasks through advances in image tokenization and training data augmentation.

Similarly, AR models have also shown strong potential in various 3D shape synthesis tasks. By sequentially predicting the “next token”, these models are designed to capture the underlying structure of 3D geometry [11, 53, 57, 60, 75, 87]. However, current AR methods for 3D generation typically operate at the level of individual voxels, triangles, or point coordinates, which introduces several significant challenges. First, the computational costs of predicting a large number of granular tokens can quickly become prohibitive, especially for complex, high-resolution 3D shapes. This computational burden limits the scalability and practicality of these models. Secondly, the focus on predicting local token-level details can result in a loss of context and global coherence, making it difficult to preserve the essential geometric structure during the generation process. For these reasons, most recent efforts have focused on diffusion-based models for 3D shape generation [12, 25, 26, 38, 70, 72].

In this paper, we propose 3D Hierarchical Wavelet-Guided Autoregressive Generation (3D-WAG) to facilitate autoregressive generation of coherent but detailed 3D shapes. 3D-WAG encodes shapes as multi-scale wavelet token maps and employs a Transformer-based architecture to predict the “next higher-resolution token map” in an autoregressive setting. The autoregressive model is trained to generate the wavelet tokens from the coarsest $1 \times 1 \times 1$ token map, and then progressively expands in resolution: at each step, the Transformer predicts the next higher-resolution token map conditioned on all the previous ones. By framing the generation task in this hierarchical, coarse-to-fine fashion, 3D-WAG sidesteps the computational burdens of traditional token-level prediction models. Also rather than fragmenting the geometry through local token prediction, our hierarchical approach synthesizes high-fidelity 3D shapes while preserving the global structure and fine-grained details. We showcase through comprehensive evaluations that 3D-WAG achieves state-of-the-art performance on widely used 3D benchmarks, outperforming existing generative models in key metrics such as Coverage, MMD, and 1-NNA. Furthermore, We also demonstrate the 3D-WAG framework’s flexibility in handling complex tasks like category conditioned generation and text-conditioned generation with compelling results.

In summary, our key contributions include:

1. The exploration of autoregressive next-scale prediction-based generation of 3D shapes, with the introduction of the 3D-WAG framework.
2. Leveraging wavelets for efficient AR modeling of high-resolution 3D shapes.
3. Extensive experimental evaluation demonstrating the superior performance and efficiency of 3D-WAG compared to existing 3D generative models, including diffusion approaches.
4. Demonstrating 3D-WAG’s generalization capabilities to class and text-conditional generation.

2. Related Work

Neural networks have increasingly shown transformative potential in 3D applications, contributing to advancements in areas such as shape modeling, scene reconstruction, and virtual simulation [23, 29, 40, 41, 50, 52, 83, 84, 86, 95, 98, 100–102]. Building on this momentum, our work focuses on generating implicit functions, which notoriously are efficient 3D data representations. In particular, by leveraging discretized signed distance functions (SDFs) and unsigned distance functions (UDFs), we aspire to enhance the fidelity and versatility of shape generation, contributing to a robust and scalable foundation for 3D shape generation.

2.1. Neural Implicit Representations

Neural Implicit Functions (NIFs) have rapidly become influential in surface reconstruction [51, 55, 63], novel view synthesis [56, 58], and image super-resolution [4, 73]. These techniques use neural networks to encode shapes and scenes, typically through SDFs [14, 63] or binary occupancy fields [55, 64], producing meshes via the marching cubes algorithm [45]. Early works like DeepSDF and OccNet [55, 63] introduced global latent codes and MLP-based decoders to represent 3D shapes using occupancy fields or signed distances. Subsequent approaches [28, 64] improved these by incorporating local latent codes to capture detailed geometry. More recent innovations, such as PCP [49] and OnSurf [48], further enhance NIFs by leveraging predictive context and on-surface priors, substantially increasing their representational power for finer geometric accuracy.

While occupancy fields and signed distance functions are effective for modeling closed shapes, recent methods have shifted towards neural unsigned distance fields (UDFs) [9, 13, 43, 44, 82, 97, 99] to model non-watertight surfaces effectively. For example, Neural Distance Fields (NDF) [13] introduced a hierarchical neural network that learns UDFs via distance-based supervision. Another approach, GIFS [89], learns shape representations by modeling query relationships to achieve UDF representation. Other recent work, such as CAP-UDF [97] and LevelSe-

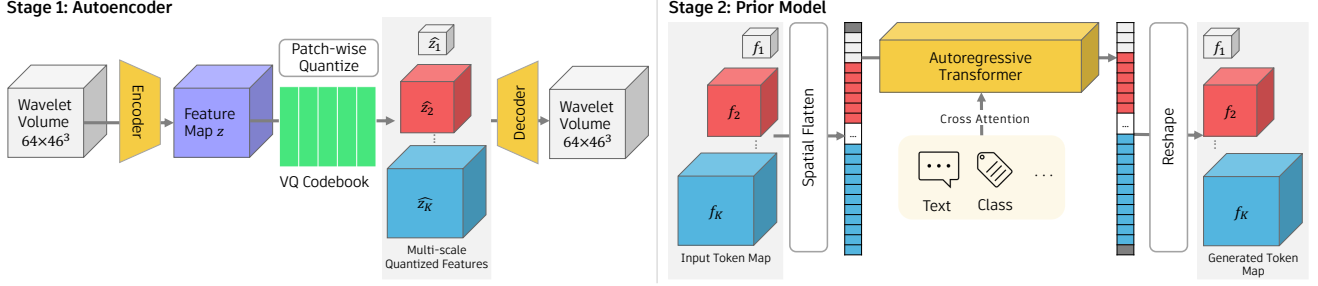


Figure 2. Overview of our architecture. We follow a two-stage training approach that is standard with latent generative models. In Stage 1, we train a vector-quantized autoencoder (VQ-VAE) on the wavelet volumes with multi-scale patch-wise quantization [78] in the latent space giving us quantized feature maps $\hat{z}_1, \hat{z}_2, \dots, \hat{z}_K$. In Stage 2, the multi-scale VQ-VAE codebook indices in the form of token maps f_1, f_2, \dots, f_K are flattened and learned with an autoregressive decoder-only Transformer prior model, enabling next-scale generation. During inference, the generated token maps are reshaped and mapped to obtain multi-scale quantized features by using codebook. Then the obtained features are converted into wavelet volumes by the decoder from Stage 1. The wavelet volumes can be further converted into implicit functions using wavelet inversion.

tUDF [99], has further refined UDF modeling by incorporating consistency-aware constraints and level-set projections. These techniques improve the optimization of UDFs, enabling accurate and detailed geometry representation. Similar to these approaches, we leverage distance fields to implicitly represent 3D shapes.

2.2. 3D Generative Models

Generating 3D content is the cornerstone of many applications like augmented/virtual reality and has been widely explored in the past few years. Early methods extended the success of models originally developed for image generation—such as GANs [18], VAEs [32], and flow-based models [31]—into the 3D domain. These models were used to generate 3D shapes in the formats like point clouds [6, 27, 39, 61, 88] and voxel grids [74, 85].

Recently, diffusion models have dominated the field of 3D shape generation [12, 25, 26, 38, 70, 72]. Several methods combine diffusion approaches with implicit representations to achieve high fidelity, producing either signed distance fields [15, 19, 25, 26, 34] or occupancy fields [94], from which meshes are extracted using marching cubes [45]. To improve training efficiency, models like Diffusion-SDF [15] and 3D-LDM [59] employ VAEs for transforming shapes into latent codes for diffusion, while Make-A-Shape [26] uses a compact wavelet-based representation to process extensive 3D datasets. Despite their advantages, diffusion models still face challenges with training stability and exhibit slower inference times due to the iterative nature of the diffusion process, which poses a significant limitation for practical applications.

AR models have achieved remarkable progress in 2D image generation [17, 68, 81], and to a noticeable extent in 3D tasks [11, 57, 60, 75, 87]. Autoregressive (AR) models are probabilistic generative methods with a tractable density,

allowing them to decompose sample likelihoods into conditional probabilities. In contrast, Generative Adversarial Networks (GANs) lack a tractable density, which prevents such factorization. However, most 3D AR models struggle with generating high-quality and high-resolution shapes due to the challenges of representation learning with higher fidelity. Particularly, we notice two recent works [57, 87] that share similar insights of utilizing AR models for 3D tasks. [87] introduces a sparse representation to only quantize non-empty grids in 3D space, but still follows a monotonic row-major order. [57] presents a non-sequential design to break the orders, but performs on all volumetric grids. Unlike prior approaches that address individual limitations through complex architectural modifications, our method leverages Transformers’ flexibility to support both unconditional and conditional generation through simple condition concatenation, achieving faster inference and better control.

3. Wavelet Autoregressive Shape Generation

Our 3D-WAG approach generates high resolution 3D shapes by leveraging a compact wavelet representation along with a Transformer-based autoregressive model, that predicts multi-scale wavelet token maps in a coarse-to-fine manner. We employ a wavelet-based representation to encode high-resolution shapes compactly, with minimal loss of detail (Sec. 3.1). An autoencoder is trained to encode the wavelet coefficients of 3D shapes into discrete, multi-scale token maps for autoregressive modeling (Sec. 3.2). We then use a Transformer-based AR model to generate these token maps, predicting the next higher-resolution map conditioned on all previous ones (Sec. 3.3). An overview of our complete 3D-WAG framework is provided in Figure 2. This multi-scale, hierarchical generation strategy built upon wavelet encodings represents a fundamental paradigm shift

from prior 3D shape synthesis techniques, especially in 3D AR approaches.

3.1. Compact Wavelet Representations

Modeling high-resolution 3D data in AR setting presents several challenges compared to their 2D image counterparts. The additional third spatial dimension exponentially increases the number of input variables that the model must learn, resulting in a dramatic increase in network parameters and memory-intensive feature maps. This increased computational overhead on GPUs, significantly limits the resolution of the modeled 3D shapes and prolongs training times. Furthermore, scaling generative models to 3D introduces complex data handling issues: the storage and processing of 3D data have substantially higher *IO* costs like download times for each training iteration.

Recently, methods like [25, 26, 71] adapted wavelet compression representation to generate high-resolution 3D shapes using diffusion models. Building on existing methods, we employ a compact wavelet-based spatial frequency representation to efficiently consume, high-resolution SDF generation in our auto-regressive framework. We use multi-scale wavelet transform to encode shape data, capturing both low and high-frequency information. We then selectively identify and retain the most information-rich wavelet detail coefficients in the high-frequency subbands. This allows our representation to compactly include a greater degree of shape details while being memory efficient. Following this we rearrange the multi-scale wavelet-tree representation into a low-resolution spatial grid format. This restructuring enables the efficient use of 3D convolutional operations to process the wavelet-based representation. While SDF grids suit only watertight meshes, wavelet representation accommodates varied implicit spatial representations. We also test UDFs to model non-watertight surfaces, like those in the DeepFashion3D dataset [104]. Inspired by UDiff [103], we also optimize wavelet filter parameters to improve the expressibility of the wavelet volume. Once learned, these parameters allow efficient encoding of surfaces in the spatial frequency domain, retaining shape details in a compact form. In Table 1, we show a quantitative comparison of the computational burden, measured in Multiply-Accumulate Operations (MACs), for a single 3D convolution applied to different shape representations with output channels of convolution equals to one. The table compares implicit and wavelet-based representations at the same input voxel resolution, demonstrating the computational efficiency of the wavelet-based approach.

3.2. Multi-Scale Wavelet Tokenization

To perform generative AR modeling through next-token prediction, we need to first break down each data instance into multiple discrete tokens. This tokenization process rep-

Table 1. **Computational burden of 3D convolutions for implicit and wavelet representations.** The implicit representation (1, 256, 256, 256) has approximately 3 times more MACs than the wavelet representation (64, 46, 46, 46).

Representation Type	Channels	Filter Size	Approx. MACs
Implicit Representation (1, 256, 256, 256)	1	$3 \times 3 \times 3$	453 million
Wavelet Representation (64, 46, 46, 46)	64	$3 \times 3 \times 3$	168 million

resents the data as a sequence of token indices. Then, a specific 1D ordering of these tokens must be established to enable the model to learn a unidirectional pattern. Predicting each token in the sequence based on its predecessors allows for coherent and context-aware generation. For non-sequential 1D data, such as 3D shapes, directly flattening spatial features into sequences for autoregressive modeling can disrupt the data’s inherent spatial structure. This naïve flattening approach weakens the natural correlations between neighboring features, ignoring the original spatial relationship. As a result, the model struggles to maintain spatial coherence, leading to less accurate representations and diminishing the overall quality of shape generation. To overcome these limitations, we formulate 3D shape generation as a hierarchical prediction task where the model estimates wavelet token maps at progressively higher resolutions. To enable this multi-scale generation process, we first train a specialized quantization autoencoder that encodes each 3D shape into K discrete token maps of varying resolutions. This multi-scale discretization allows us to represent shapes at different levels of detail, from coarse structural information in low-resolution token maps to fine geometric details in high-resolution ones.

For each shape S in the training dataset, an autoencoder learns to compress the continuous wavelet coefficients into a discrete vocabulary of multi-scale token maps while preserving the essential shape information at each scale. The input for the autoencoder is a wavelet representation W created using wavelet filters mentioned in Sec. 3.1. The autoencoder transforms the input W into multi-scale discrete token maps $F = (f_1, f_2, \dots, f_K)$. Here f_1 and f_K represent the token maps of the coarsest and finest scales respectively. Our approach utilizes a 3D convolutional variational autoencoder architecture with a modified multi-scale quantization layer. Our multi-scale quantization **Encoding** and **Reconstruction** algorithms, inspired by the approaches of [36, 78], are described below. In the quantization process, each token map f_k is dependent only on its preceding token maps $(f_1, f_2, \dots, f_{k-1})$, which contributes to a progressive and coherent multi-scale representation. To ensure consistency across scales, we employ a shared codebook Z . This design allows our model to effectively capture and reconstruct multi-scale information across various res-

olutions, preserving critical details in autoregressive shape generation.

Encoding: The multi-scale vector quantization encoding algorithm progressively encodes an input shape across multiple resolutions, leveraging residual connections to capture details at different scales. Given a wavelet encoding W , the algorithm uses an encoder E to obtain an initial feature map z . It then iteratively quantizes this feature map over K steps, where each step corresponds to a predefined resolution (h_k, w_k, d_k) . At each scale k , the algorithm interpolates current residual tensor z_k^{res} to match the current resolution (h_k, w_k, d_k) . At level K , z_K^{res} is initialized with z . The interpolated tensors at every scale is quantized using the function proposed in [69] to obtain the quantized token maps f_k . The quantized token maps f_k are used to retrieve feature vectors from the codebook to create quantized feature representation \hat{z}_k^{res} . The quantized feature representation \hat{z}_k^{res} is a quantized estimate of the tensor z_k^{res} . Then, \hat{z}_k^{res} is upsampled back to the original scale. Residual is computed by subtracting the decoded quantized features $C_k(\hat{z}_k^{res})$, from the feature map z_k^{res} , which becomes z_{k-1}^{res} . We continue this process for all the scales. C_k represents a convolutional layer for scale k and mitigates information loss during upscaling z_k to resolution $h_K \times w_K \times d_K$. No convolutional layers are used while downsampling z . This recursive process produces a sequence of multi-scale tokens F , encapsulating hierarchical and multi-resolution information from the wavelet encodings.

Reconstruction: The multi-scale reconstruction algorithm reverses the encoding process to reconstruct a wavelet encoding from the multi-scale token maps generated during encoding. Given a sequence of multi-scale token maps F , the algorithm iteratively reconstructs a feature map \hat{z}^{recon} by decoding information at progressively finer scales. The process starts by initializing \hat{z}^{recon} to zero. For each scale k in the sequence of K steps, the algorithm retrieves the quantized representation f_k from F . It then uses a codebook(Z) lookup to obtain a latent representation z_k^{recon} , corresponding to the token map f_k . This latent representation z_k^{recon} is then interpolated to match the current resolution (h_k, w_k, d_k) . A residual addition between current estimate \hat{z}^{recon} and $C_k(z_k^{recon})$ become the new \hat{z}^{recon} estimate. Once all scales are processed, a decoder D is applied to \hat{z}^{recon} to produce the final reconstructed wavelet volume \hat{W} .

The autoencoder is trained by minimizing the reconstruction error between the wavelet representation W and its reconstruction \hat{W} . Additionally, a commitment loss is minimized to ensure that the encoder reliably commits to a specific embedding, stabilizing its output. Thus, the total

training objective L becomes:

$$L = \lambda_{recon} \|W - \hat{W}\|_2 + \lambda_{commit} \sum_1^K \|z_k^{res} - \hat{z}_k^{res}\|_2, \quad (1)$$

Where $(\lambda_{recon}, \lambda_{commit})$ are hyperparameters that represent the weights of the reconstruction error and commitment loss terms respectively.

3.3. Next-scale Generative Model

The token map encodings, learned during the first stage of training, are used to train an autoregressive shape generation model. The goal of this model is to generate token maps $\{f_1, f_2, \dots, f_K\}$ using a “next-scale prediction” approach. Starting with a random initial token map, the model generates subsequent token maps one step at a time, each at progressively higher resolutions. This process continues until it reaches f_K , which matches the resolution of the original feature map. To accomplish this, we use GPT-2 [66] style decoder-only Transformer model. The autoregressive likelihood is defined as $p(f) = \prod_{i=1}^K p(f_i | f_{<i})$, where each f_i is conditioned on all preceding token maps $f_{<i}$.

It is important to note that, at each step, all token maps at the current scale are estimated simultaneously rather than sequentially. For class-conditional wavelet synthesis, we use a class embedding as the start token, denoted by $[s]$, which also serves as the conditioning factor for AdaLN. Additionally, we normalize the queries and keys to unit vectors before the attention mechanism, enhancing training stability in our generative model. The cross-entropy loss L_{CE} is used for the autoregressive shape generation:

$$L_{CE} = - \sum_{i=1}^K \log p(f_i | f_{<i}), \quad (2)$$

where $p(f_i | f_{<i})$ is the predicted probability of the i -th token map f_i given all previous token maps $f_{<i}$. This loss function encourages the model to assign high probabilities to the correct token map f_i at each step, ensuring accurate autoregressive generation by minimizing the negative log-likelihood of the true token maps.

During autoregressive inference, multi-scale token maps are sampled progressively, capturing spatial details at increasing resolutions. This sequential process enables the model to coherently generate complex shapes, refining details at each scale to produce a realistic output. These token maps are transformed into wavelet reconstruction \hat{W} using **Reconstruction** algorithm presented in Sec. 3.2. This wavelet representation is inverted using an inverse wavelet transformation to generate an implicit representation of the shape. Additional design choices of our approach and details of shape retrieval from wavelet representation are discussed in Appendix.

We note that, in the 3D case, generating a volume token sequence $\{f_1, f_2, \dots, f_K\}$ with a conventional self-attention Transformer requires $\mathcal{O}(n^3)$ autoregressive steps and incurs a computational cost of $\mathcal{O}(n^9)$. By employing the 3D-WAG approach, the time complexity for generating a shape with an $n \times n \times n$ latent representation is substantially reduced to $\mathcal{O}(n^6)$, see Appendix for proof.

4. Experiments

In this section, we evaluate the effectiveness of our approach in shape generation in the unconditional (Sec. 4.1) and conditional (Sec. 4.2) setting. Finally, in Sec. 4.3, we perform ablation studies on the number of scales and the choice of quantization techniques to assess their impact on shape generation.

4.1. Shape Generation

Dataset and Metrics. For our evaluations, we consider the DeepFashion3D dataset [104] and the ShapeNet dataset [7]. The DeepFashion3D dataset includes 1,798 3D garment models from 563 unique items across 10 categories. We randomly split this dataset into 80% for training and 20% for testing. We model the shapes using distance fields with a voxel resolution of 256^3 . On both datasets, we present our model’s performance on unconditional generation using the Coverage (COV), Minimum Matching Distance (MMD), and 1-Nearest Neighbor Classifier Accuracy (1-NNA) metrics. Following previous art, to compute these metrics we generate 1000 shapes for DeepFashion3D and 2000 for ShapeNet, then sample 2048 points on the surfaces. For the ShapeNet dataset, following [25, 34], we compute metrics on the airplane and chair categories, while we train using the entire dataset for qualitative evaluation.

Results on ShapeNet. We present our results on ShapeNet dataset in Table 2. We compare our 3D-WAG model against previous methods, including UDiff [103], IM-GAN [10], Voxel-GAN [33], PointDiff [46], SPAGHETTI [20], WaveGen [25], and SALAD [34]. We also evaluate our approach in comparison to the autoregressive approach ImAM [47], which follows token-by-token prediction to generate shapes.

Our model outperforms the state-of-the-art in shape generation on the ShapeNet dataset. Specifically, we obtained improved Coverage (COV) and Minimum Matching Distance (MMD) across the Chair and Airplane categories. For instance, in the Chair category, 3D-WAG achieves a COV score of 57.30 and an MMD score of 10.90 (CD), surpassing the next-best model by a significant margin. Similarly, in the Airplane category, 3D-WAG reaches a COV of 66.80 and a notably low MMD score of 2.900 (CD), again outperforming other methods. This improvement in COV indicates that 3D-WAG generates a broader variety of realistic shapes, while the low MMD reflects high fidelity to real

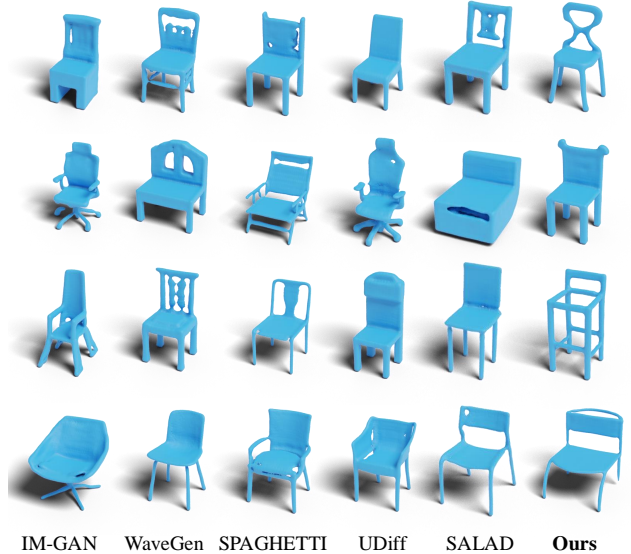


Figure 3. Qualitative comparison of 3D chair generation results across various methods on the ShapeNet dataset. Models shown include IM-GAN, WaveGen, SPAGHETTI, UDiff, and SALAD, with our method (3D-WAG) on the far right. Our method demonstrates improved structural coherence, finer details, and a wider diversity of generated chair designs, capturing both simple and complex geometries more effectively than competing methods.

data. The model’s autoregressive next-scale token map prediction strategy contributes to these gains by efficiently handling high-resolution details without compromising computational efficiency, as highlighted by the favorable inference time in Table 2. Additionally, 3D-WAG achieves favorable 1-Nearest Neighbor Classifier Accuracy (1-NNA) scores, indicating that generated shapes are distinct from training samples and capture novel variations. Overall, these results validate the effectiveness of our approach in advancing the fidelity, diversity, and faster inference in 3D shape generation. In Fig. 3, we compare the qualitative results of our method and state-of-the-art methods.

Results on DeepFashion3D. As diffusion models are recently most used for shape generation, we compare our approach with SOTA diffusion-based shape generation models, including UDiff [103], PointDiff [46], WaveGen [25], Diffusion-SDF [15], LAS-Diffusion [96]. Each model is evaluated with the official implementations. WaveGen [25] and UDiff [103] are also based on wavelet input representation ensuring a fair comparison. Table 3 highlights the superior performance of 3D-WAG on the DeepFashion3D dataset compared to previous approaches. 3D-WAG achieves the highest Coverage (COV) scores, with 69.85 (CD) and 68.03 (EMD), indicating a broader diversity of generated shapes that better represent the dataset’s range of 3D garments. Additionally, 3D-WAG excels in Minimum Matching Distance (MMD), achieving the lowest scores

Table 2. **Comparison of shape generation performance and time under ShapeNet dataset.** Inference time is reported in seconds. MMD-CD and MMD-EMD scores are scaled by 10^3 and 10^2 , respectively.

Method	COV \uparrow		Chair MMD \downarrow		1-NNA \downarrow		COV \uparrow		Airplane MMD \downarrow		1-NNA \downarrow		Time (s)
	CD	EMD	CD	EMD	CD	EMD	CD	EMD	CD	EMD	CD	EMD	
IM-GAN [10]	57.01	55.23	12.02	14.76	62.15	63.78	62.21	63.10	3.298	8.479	76.50	76.29	2.98
Voxel-GAN [33]	44.29	39.89	15.35	17.59	80.74	81.62	39.01	39.78	5.875	11.53	93.60	92.98	2.75
PointDiff [46]	51.88	56.11	12.92	16.35	62.02	63.95	60.55	62.71	3.615	9.620	74.98	72.63	—
SPAGHETTI [20]	50.11	50.73	15.02	16.05	72.82	69.93	57.30	59.12	4.342	9.021	79.84	79.33	27.4
SALAD (Global) [34]	50.13	49.12	11.93	14.35	63.25	61.73	55.42	59.85	3.891	9.073	82.61	80.87	33.2
SALAD [34]	56.91	55.65	11.89	14.50	58.23	58.90	63.65	65.82	3.721	8.329	74.35	71.52	38.0
WaveGen [25]	50.12	50.67	12.31	14.47	65.58	63.39	61.40	59.57	3.605	8.075	76.23	73.25	15.4
ImAM [47]	54.38	55.71	11.90	13.97	62.43	62.11	65.82	65.41	3.248	7.900	77.12	79.13	14.2
UDiff [103]	53.02	56.51	11.82	14.19	66.42	63.91	65.23	64.22	3.229	7.879	74.85	79.42	39.0
Ours	57.30	58.41	10.90	13.06	68.10	66.31	66.80	65.93	2.900	7.543	82.10	80.92	2.50

Table 3. **Comparison of shape generation under DeepFashion3D dataset.** MMD-CD scores and MMD-EMD scores are scaled by 10^3 and 10^2 , respectively.

Method	COV \uparrow		MMD \downarrow		1-NNA \downarrow	
	CD	EMD	CD	EMD	CD	EMD
PointDiff [46]	68.90	64.89	11.20	15.72	83.50	87.93
WaveGen [25]	62.75	52.15	15.78	17.29	93.20	94.96
Diffusion-SDF [15]	67.45	62.40	14.92	16.88	89.31	92.81
LAS-Diffusion [96]	67.82	56.43	14.75	16.79	88.95	91.68
UDiff [103]	69.98	68.01	11.75	14.25	82.11	82.47
Ours	69.85	68.03	10.96	13.89	82.01	82.30

across both CD and EMD metrics, with values of 10.96 and 13.89, respectively, demonstrating higher fidelity to real shapes. The 1-Nearest Neighbor Accuracy (1-NNA) scores of 82.01 (CD) and 82.30 (EMD) further confirm that 3D-WAG produces realistic samples with a similarity distribution close to the real data. These results validate the effectiveness of our approach in open-surface shape generation in terms of both diversity and quality. The model’s performance establishes it as a new benchmark for 3D garment generation on DeepFashion3D, showcasing its ability to capture complex geometries and fine details with improved efficiency and fidelity. Fig. 4 presents qualitative examples of our unconditional generation results on DeepFashion3D. More unconditional generation results, as well as examples of failure cases, can be found in the Appendix.

4.2. Conditional Generation

Leveraging cross-attention mechanisms, we explore two applications of our autoregressive Transformer model: class-conditional generation and text-conditional generation, each utilizing annotated data during training to guide the generation process. In the class-conditional setting, we trained our model on 15 categories from the ShapeNet dataset, allowing it to generate shapes aligned with specific classes. Results for this class-conditional generation task are shown in Figure 5, showcasing the model’s ability to produce category-specific shapes with diverse details.

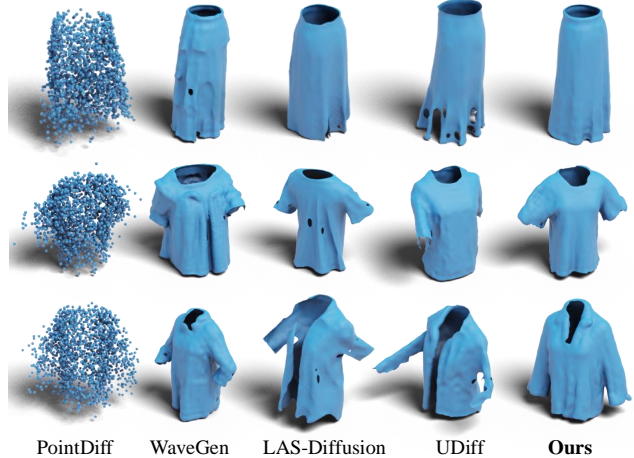


Figure 4. Qualitative comparison of 3D garment generation results on the DeepFashion3D dataset [104], comparing PointDiff, WaveGen, LAS-Diffusion, UDiff, and our method (3D-WAG) on the far right. Our approach produces more coherent and realistic garment shapes, capturing intricate structural details such as folds, sleeves, and openings with higher fidelity than other methods.

We also fine-tuned the AR Transformer with text annotations using CLIP encoder to generate shapes using text prompts guidance on small ShapeNet and DeepFashion3D subsets. The resulting meshes can then be textured using the text input to produce realistic 3D assets. In this work, we employed Text2Tex model [8] to generate textures. We showcase our results on the text-conditional generation task in Fig. 1 and 6. Although these results were obtained from a limited dataset, they reveal the potential of our method. Future work will involve scaling this approach to a larger dataset, which would allow for a more comprehensive evaluation to further validate the model’s robustness.

4.3. Ablation Studies

We present a comprehensive ablation study examining the influence of several key components in our generation pro-

Table 4. **Comparison of shape generation on planes dataset with different number of token maps (in the brackets).** MMD-CD and MMD-EMD scores are scaled by 10^3 and 10^2 .

Method	COV \uparrow		MMD \downarrow		1-NNA \downarrow	
	CD	EMD	CD	EMD	CD	EMD
Ours (4 scales)	65.98	65.32	3.081	7.613	82.94	81.34
Ours (11 scales)	66.80	65.93	2.900	7.543	82.10	80.92

cess. First, we investigate the effect of varying the number of token maps or stages, evaluating how this choice impacts the overall generation quality. Next, we explore the impact of different quantization techniques to assess their effect on generation performance, providing insight into how quantization impacts the generation capability.

Varying number of token maps or scales. The results in Table 4 demonstrate the impact of scaling the number of token maps used in the 3D-WAG generation process. Using 11 token maps, the baseline 3D-WAG model achieves the highest Coverage (COV) scores of 66.80 and 65.93 for CD and EMD metrics respectively. When reducing the number of token maps to 4, we observe a slight degradation in performance across the board. The COV scores drop to 65.98 (CD) and 65.32 (EMD), indicating a minor decrease in shape diversity coverage. The MMD scores also increase from 2.900 to 3.081 (CD) and 7.543 to 7.613 (EMD), suggesting a small decline in distribution matching quality. However, the 1-NNA scores remain strong at 82.10 (CD) and 81.34 (EMD) even with the reduced token maps. This implies that the generated shapes maintain high fidelity and avoid mode collapse, despite the modest performance drop in other metrics. The results highlight the flexibility of the 3D-WAG approach, where the number of token maps can be adjusted to balance generation quality and computational complexity. While the full 11 token map configuration offers the best overall performance, the 4 token map variant still delivers compelling results, making it a viable option for resource-constrained deployments. This adaptability underscores the versatility of our framework.

Comparison with different quantization techniques. In our experiments Nearest Neighbor(NN) quantization [69] demonstrates superior performance across multiple evaluation metrics compared to other quantization-based approaches. As shown in Table 5, NN quantization method achieves the highest Coverage (COV) scores of 66.80 and 65.93 for CD and EMD metrics respectively, outperforming variants with LFQ [92] and FSQ [54]. Furthermore, NN quantization exhibits lower MMD scores (2.900 and 7.543 for CD and EMD), indicating better overall distribution matching between generated and real shapes.

5. Conclusion

In this paper, we present 3D-WAG, a novel autoregressive approach for 3D shape generation that transforms the tra-

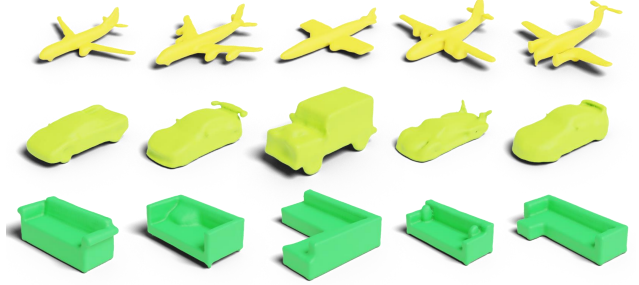


Figure 5. Examples of shape generation conditioned by class: airplane (top), car (middle), and sofa (bottom) categories. Our model produces realistic and varied shapes within each category.



Figure 6. Examples of our text-conditioned shape generation. The results show our approach generating globally coherent output that follows the input text condition.

Table 5. **Comparison of shape generation on planes dataset with our method with different quantization techniques.** MMD-CD and MMD-EMD scores are scaled by 10^3 and 10^2 .

Method	COV \uparrow		MMD \downarrow		1-NNA \downarrow	
	CD	EMD	CD	EMD	CD	EMD
Ours	66.80	65.93	2.900	7.543	82.01	80.92
Ours + LFQ	63.90	64.29	3.310	7.917	79.4	82.30
Ours + FSQ	65.5	64.87	3.109	7.840	79.20	79.88

ditional “next-token” prediction framework of 3D AR approaches. By representing shapes as multi-scale wavelet token maps and employing a transformer to autoregressively predict the “next higher-resolution token map,” our method effectively addresses the computational challenges inherent to large-scale 3D generative modeling. The key innovation of 3D-WAG is in reframing 3D autoregressive generation as a “next-scale” prediction task, allowing for efficient generation while preserving intricate geometric details in a structured, hierarchical fashion. This approach is validated by 3D-WAG’s outstanding performance on widely recognized benchmarks, where it achieves superior Coverage and MMD metrics compared to state-of-the-art models. Beyond unconditional generation, 3D-WAG proves highly versatile, handling class and text-conditioned shape generation with ease. Our results demonstrate that 3D-WAG produces high-fidelity 3D shapes closely aligned with real data distributions while delivers faster inference times.

Future Work. While the current work mainly focuses on reporting a viable new approach that competes

with established 3D methods, we plan to optimize it and test its scalability properties on large datasets. Additionally, future works will explore a broader range of applications, potentially enabling more complex 3D generation and investigate alternative conditioning mechanisms to further enhance the flexibility and robustness of 3D-WAG across diverse 3D tasks.

References

- [1] Josh Achiam, Steven Adler, Sandhini Agarwal, Lama Ahmad, Ilge Akkaya, Florencia Leoni Aleman, Diogo Almeida, Janko Altenschmidt, Sam Altman, Shyamal Anadkat, et al. Gpt-4 technical report. *arXiv preprint arXiv:2303.08774*, 2023. 1
- [2] Rohan Anil, Andrew M Dai, Orhan Firat, Melvin Johnson, Dmitry Lepikhin, Alexandre Passos, Siamak Shakeri, Emanuel Taropa, Paige Bailey, Zhifeng Chen, et al. Palm 2 technical report. *arXiv preprint arXiv:2305.10403*, 2023. 1
- [3] Jinze Bai, Shuai Bai, Yunfei Chu, Zeyu Cui, Kai Dang, Xiaodong Deng, Yang Fan, Wenbin Ge, Yu Han, Fei Huang, et al. Qwen technical report. *arXiv preprint arXiv:2309.16609*, 2023. 1
- [4] Tim Brooks, Aleksander Holynski, and Alexei A Efros. Instructpix2pix: Learning to follow image editing instructions. In *Proceedings of the IEEE/CVF Conference on Computer Vision and Pattern Recognition*, pages 18392–18402, 2023. 2
- [5] Tom B Brown. Language models are few-shot learners. *arXiv preprint arXiv:2005.14165*, 2020. 1, 2
- [6] Ruojin Cai, Guandao Yang, Hadar Averbuch-Elor, Zekun Hao, Serge Belongie, Noah Snaveley, and Bharath Hariharan. Learning gradient fields for shape generation. In *Computer Vision—ECCV 2020: 16th European Conference, Glasgow, UK, August 23–28, 2020, Proceedings, Part III 16*, pages 364–381. Springer, 2020. 3
- [7] Angel X Chang, Thomas Funkhouser, Leonidas Guibas, Pat Hanrahan, Qixing Huang, Zimo Li, Silvio Savarese, Manolis Savva, Shuran Song, Hao Su, et al. Shapenet: An information-rich 3D model repository. *arXiv preprint arXiv:1512.03012*, 2015. 6, 15, 16, 17
- [8] Dave Zhenyu Chen, Yawar Siddiqui, Hsin-Ying Lee, Sergey Tulyakov, and Matthias Nießner. Text2tex: Text-driven texture synthesis via diffusion models. *arXiv preprint arXiv:2303.11396*, 2023. 7
- [9] Weikai Chen, Cheng Lin, Weiyang Li, and Bo Yang. 3psdf: Three-pole signed distance function for learning surfaces with arbitrary topologies. In *Proceedings of the IEEE/CVF Conference on Computer Vision and Pattern Recognition*, pages 18522–18531, 2022. 2
- [10] Zhiqin Chen and Hao Zhang. Learning implicit fields for generative shape modeling. In *Proceedings of the IEEE/CVF Conference on Computer Vision and Pattern Recognition*, pages 5939–5948, 2019. 6, 7
- [11] An-Chieh Cheng, Xueting Li, Sifei Liu, Min Sun, and Ming-Hsuan Yang. Autoregressive 3d shape generation via canonical mapping. *arXiv preprint arXiv:2204.01955*, 2022. 2, 3
- [12] Yen-Chi Cheng, Hsin-Ying Lee, Sergey Tulyakov, Alexander G Schwing, and Liang-Yan Gui. Sdfusion: Multimodal 3d shape completion, reconstruction, and generation. In *Proceedings of the IEEE/CVF Conference on Computer Vision and Pattern Recognition*, pages 4456–4465, 2023. 2, 3
- [13] Julian Chibane, Gerard Pons-Moll, et al. Neural unsigned distance fields for implicit function learning. *Advances in Neural Information Processing Systems*, 33:21638–21652, 2020. 2
- [14] Gene Chou, Ilya Chugunov, and Felix Heide. Gensdf: Two-stage learning of generalizable signed distance functions. In *Advances in Neural Information Processing Systems*, 2022. 2
- [15] Gene Chou, Yuval Bahat, and Felix Heide. Diffusion-sdf: Conditional generative modeling of signed distance functions. In *Proceedings of the IEEE/CVF International Conference on Computer Vision*, pages 2262–2272, 2023. 3, 6, 7
- [16] Aakanksha Chowdhery, Sharan Narang, Jacob Devlin, Maarten Bosma, Gaurav Mishra, Adam Roberts, Paul Barham, Hyung Won Chung, Charles Sutton, Sebastian Gehrmann, et al. Palm: Scaling language modeling with pathways. *Journal of Machine Learning Research*, 24(240): 1–113, 2023. 1
- [17] Patrick Esser, Robin Rombach, and Bjorn Ommer. Taming transformers for high-resolution image synthesis. In *Proceedings of the IEEE/CVF Conference on Computer Vision and Pattern Recognition*, pages 12873–12883, 2021. 3, 14
- [18] Ian Goodfellow, Jean Pouget-Abadie, Mehdi Mirza, Bing Xu, David Warde-Farley, Sherjil Ozair, Aaron Courville, and Yoshua Bengio. Generative adversarial networks. *Communications of the ACM*, 63(11):139–144, 2020. 3
- [19] Anchit Gupta, Wenhan Xiong, Yixin Nie, Ian Jones, and Barlas Oğuz. 3dgen: Triplane latent diffusion for textured mesh generation. *arXiv preprint arXiv:2303.05371*, 2023. 3
- [20] Amir Hertz, Or Perel, Raja Giryes, Olga Sorkine-Hornung, and Daniel Cohen-Or. Spaghetti: Editing implicit shapes through part aware generation. *ACM Transactions on Graphics (TOG)*, 41(4):1–20, 2022. 6, 7
- [21] Jordan Hoffmann, Sebastian Borgeaud, Arthur Mensch, Elena Buchatskaya, Trevor Cai, Eliza Rutherford, Diego de Las Casas, Lisa Anne Hendricks, Johannes Welbl, Aidan Clark, et al. Training compute-optimal large language models. *arXiv preprint arXiv:2203.15556*, 2022. 1
- [22] Fei Hou, Xuhui Chen, Wencheng Wang, Hong Qin, and Ying He. Robust zero level-set extraction from unsigned distance fields based on double covering. *arXiv preprint arXiv:2310.03431*, 2023. 16
- [23] Han Huang, Yulun Wu, Junsheng Zhou, Ge Gao, Ming Gu, and Yu-Shen Liu. Neusurf: On-surface priors for neural surface reconstruction from sparse input views. In *Proceedings of the AAAI Conference on Artificial Intelligence*, 2024. 2

- [24] Lei Huang, Weijiang Yu, Weitao Ma, Weihong Zhong, Zhangyin Feng, Haotian Wang, Qianglong Chen, Weihua Peng, Xiaocheng Feng, Bing Qin, et al. A survey on hallucination in large language models: Principles, taxonomy, challenges, and open questions. *arXiv preprint arXiv:2311.05232*, 2023. 1
- [25] Ka-Hei Hui, Ruihui Li, Jingyu Hu, and Chi-Wing Fu. Neural wavelet-domain diffusion for 3d shape generation. In *SIGGRAPH Asia 2022 Conference Papers*, pages 1–9, 2022. 2, 3, 4, 6, 7
- [26] Ka-Hei Hui, Aditya Sanghi, Arianna Rampini, Kamal Rahimi Malekshan, Zhengzhe Liu, Hooman Shayani, and Chi-Wing Fu. Make-a-shape: a ten-million-scale 3d shape model. In *Forty-first International Conference on Machine Learning*, 2024. 2, 3, 4
- [27] Le Hui, Rui Xu, Jin Xie, Jianjun Qian, and Jian Yang. Progressive point cloud deconvolution generation network. In *Computer Vision—ECCV 2020: 16th European Conference, Glasgow, UK, August 23–28, 2020, Proceedings, Part XV 16*, pages 397–413. Springer, 2020. 3
- [28] Chiyu Jiang, Avneesh Sud, Ameesh Makadia, Jingwei Huang, Matthias Nießner, Thomas Funkhouser, et al. Local implicit grid representations for 3D scenes. In *Proceedings of the IEEE/CVF Conference on Computer Vision and Pattern Recognition*, pages 6001–6010, 2020. 2
- [29] Chuan Jin, Tieru Wu, and Junsheng Zhou. Multi-grid representation with field regularization for self-supervised surface reconstruction from point clouds. *Computers & Graphics*, 2023. 2
- [30] Jared Kaplan, Sam McCandlish, Tom Henighan, Tom B Brown, Benjamin Chess, Rewon Child, Scott Gray, Alec Radford, Jeffrey Wu, and Dario Amodei. Scaling laws for neural language models. *arXiv preprint arXiv:2001.08361*, 2020. 2, 17
- [31] Durk P Kingma and Prafulla Dhariwal. Glow: Generative flow with invertible 1x1 convolutions. *Advances in neural information processing systems*, 31, 2018. 3
- [32] Diederik P Kingma and Max Welling. Auto-encoding variational bayes. *arXiv preprint arXiv:1312.6114*, 2013. 3
- [33] Marian Kleineberg, Matthias Fey, and Frank Weichert. Adversarial generation of continuous implicit shape representations. *arXiv preprint arXiv:2002.00349*, 2020. 6, 7
- [34] Juil Koo, Seungwoo Yoo, Minh Hieu Nguyen, and Minhyuk Sung. Salad: Part-level latent diffusion for 3d shape generation and manipulation. In *Proceedings of the IEEE/CVF International Conference on Computer Vision*, pages 14441–14451, 2023. 3, 6, 7
- [35] Teven Le Scao, Angela Fan, Christopher Akiki, Ellie Pavlick, Suzana Ilić, Daniel Hesslow, Roman Castagné, Alexandra Sasha Luccioni, François Yvon, Matthias Gallé, et al. Bloom: A 176b-parameter open-access multilingual language model, 2023. 1
- [36] Doyup Lee, Chiheon Kim, Saehoon Kim, Minsu Cho, and Wook-Shin Han. Autoregressive image generation using residual quantization. In *Proceedings of the IEEE/CVF Conference on Computer Vision and Pattern Recognition*, pages 11523–11532, 2022. 4
- [37] Doyup Lee, Chiheon Kim, Saehoon Kim, Minsu Cho, and Wook-Shin Han. Autoregressive image generation using residual quantization. In *Proceedings of the IEEE/CVF Conference on Computer Vision and Pattern Recognition*, pages 11523–11532, 2022. 2
- [38] Muheng Li, Yueqi Duan, Jie Zhou, and Jiwen Lu. Diffusion-sdf: Text-to-shape via voxelized diffusion. In *Proceedings of the IEEE/CVF Conference on Computer Vision and Pattern Recognition*, pages 12642–12651, 2023. 2, 3
- [39] Ruihui Li, Xianzhi Li, Ka-Hei Hui, and Chi-Wing Fu. Sp-gan: Sphere-guided 3d shape generation and manipulation. *ACM Transactions on Graphics (TOG)*, 40(4):1–12, 2021. 3
- [40] Shujuan Li, Junsheng Zhou, Baorui Ma, Yu-Shen Liu, and Zhizhong Han. NeAF: Learning neural angle fields for point normal estimation. In *Proceedings of the AAAI Conference on Artificial Intelligence*, 2023. 2
- [41] Shujuan Li, Junsheng Zhou, Baorui Ma, Yu-Shen Liu, and Zhizhong Han. Learning continuous implicit field with local distance indicator for arbitrary-scale point cloud upsampling. In *Proceedings of the AAAI Conference on Artificial Intelligence*, 2024. 2
- [42] Xuantong Liu, Shaozhe Hao, Xianbiao Qi, Tianyang Hu, Jun Wang, Rong Xiao, and Yuan Yao. Elucidating the design space of language models for image generation. *arXiv preprint arXiv:2410.16257*, 2024. 2
- [43] Yu-Tao Liu, Li Wang, Jie Yang, Weikai Chen, Xiaoxu Meng, Bo Yang, and Lin Gao. Neudf: Leaning neural unsigned distance fields with volume rendering. In *Proceedings of the IEEE/CVF Conference on Computer Vision and Pattern Recognition*, pages 237–247, 2023. 2
- [44] Xiaoxiao Long, Cheng Lin, Lingjie Liu, Yuan Liu, Peng Wang, Christian Theobalt, Taku Komura, and Wenping Wang. Neuraludf: Learning unsigned distance fields for multi-view reconstruction of surfaces with arbitrary topologies. *arXiv preprint arXiv:2211.14173*, 2022. 2
- [45] William E Lorensen and Harvey E Cline. Marching cubes: A high resolution 3D surface construction algorithm. *ACM Siggraph Computer Graphics*, 21(4):163–169, 1987. 2, 3
- [46] Shitong Luo and Wei Hu. Diffusion probabilistic models for 3d point cloud generation. In *Proceedings of the IEEE/CVF Conference on Computer Vision and Pattern Recognition*, pages 2837–2845, 2021. 6, 7
- [47] Simian Luo, Xuelin Qian, Yanwei Fu, Yinda Zhang, Ying Tai, Zhenyu Zhang, Chengjie Wang, and Xiangyang Xue. Learning versatile 3d shape generation with improved ar models. *arXiv preprint arXiv:2303.14700*, 2023. 6, 7
- [48] Baorui Ma, Yu-Shen Liu, and Zhizhong Han. Reconstructing surfaces for sparse point clouds with on-surface priors. In *Proceedings of the IEEE/CVF Conference on Computer Vision and Pattern Recognition*, 2022. 2
- [49] Baorui Ma, Yu-Shen Liu, Matthias Zwicker, and Zhizhong Han. Surface reconstruction from point clouds by learning predictive context priors. In *Proceedings of the IEEE/CVF Conference on Computer Vision and Pattern Recognition*, 2022. 2

- [50] Baorui Ma, Haoge Deng, Junsheng Zhou, Yu-Shen Liu, Tiejun Huang, and Xinlong Wang. Geodream: Disentangling 2d and geometric priors for high-fidelity and consistent 3d generation. *arXiv preprint arXiv:2311.17971*, 2023. [2](#)
- [51] Baorui Ma, Yu-Shen Liu, and Zhizhong Han. Learning signed distance functions from noisy 3d point clouds via noise to noise mapping. In *International Conference on Machine Learning (ICML)*, 2023. [2](#)
- [52] Baorui Ma, Junsheng Zhou, Yu-Shen Liu, and Zhizhong Han. Towards better gradient consistency for neural signed distance functions via level set alignment. In *Proceedings of the IEEE/CVF Conference on Computer Vision and Pattern Recognition*, pages 17724–17734, 2023. [2](#)
- [53] Tejaswini Medi, Jawad Tayyub, Muhammad Sarmad, Frank Lindseth, and Margret Keuper. Fullformer: Generating shapes inside shapes. In *DAGM German Conference on Pattern Recognition*, pages 147–162. Springer, 2023. [2](#)
- [54] Fabian Mentzer, David Minnen, Eirikur Agustsson, and Michael Tschannen. Finite scalar quantization: Vq-vae made simple. *arXiv preprint arXiv:2309.15505*, 2023. [8](#)
- [55] Lars Mescheder, Michael Oechsle, Michael Niemeyer, Sebastian Nowozin, and Andreas Geiger. Occupancy networks: Learning 3D reconstruction in function space. In *Proceedings of the IEEE/CVF Conference on Computer Vision and Pattern Recognition*, pages 4460–4470, 2019. [2](#)
- [56] B Mildenhall, PP Srinivasan, M Tancik, JT Barron, R Ramamoorthi, and R Ng. NeRF: Representing scenes as neural radiance fields for view synthesis. In *European Conference on Computer Vision*, 2020. [2](#)
- [57] Paritosh Mittal, Yen-Chi Cheng, Maneesh Singh, and Shubham Tulsiani. Autosdf: Shape priors for 3d completion, reconstruction and generation. In *Proceedings of the IEEE/CVF Conference on Computer Vision and Pattern Recognition*, pages 306–315, 2022. [2](#), [3](#)
- [58] Thomas Müller, Alex Evans, Christoph Schied, and Alexander Keller. Instant neural graphics primitives with a multiresolution hash encoding. *ACM Transactions on Graphics (ToG)*, 41(4):1–15, 2022. [2](#)
- [59] Gimin Nam, Mariem Khelifi, Andrew Rodriguez, Alberto Tono, Linqi Zhou, and Paul Guerrero. 3d-ldm: Neural implicit 3d shape generation with latent diffusion models. *arXiv preprint arXiv:2212.00842*, 2022. [3](#)
- [60] Charlie Nash, Yaroslav Ganin, SM Ali Eslami, and Peter Battaglia. Polygen: An autoregressive generative model of 3d meshes. In *International Conference on Machine Learning*, pages 7220–7229. PMLR, 2020. [2](#), [3](#)
- [61] Alex Nichol, Heewoo Jun, Prafulla Dhariwal, Pamela Mishkin, and Mark Chen. Point-e: A system for generating 3d point clouds from complex prompts. *arXiv preprint arXiv:2212.08751*, 2022. [3](#)
- [62] Long Ouyang, Jeffrey Wu, Xu Jiang, Diogo Almeida, Carroll Wainwright, Pamela Mishkin, Chong Zhang, Sandhini Agarwal, Katarina Slama, Alex Ray, et al. Training language models to follow instructions with human feedback. *Advances in neural information processing systems*, 35: 27730–27744, 2022. [1](#)
- [63] Jeong Joon Park, Peter Florence, Julian Straub, Richard Newcombe, and Steven Lovegrove. DeepSDF: Learning continuous signed distance functions for shape representation. In *Proceedings of the IEEE/CVF Conference on Computer Vision and Pattern Recognition*, pages 165–174, 2019. [2](#)
- [64] Songyou Peng, Michael Niemeyer, Lars Mescheder, Marc Pollefeys, and Andreas Geiger. Convolutional occupancy networks. In *European Conference on Computer Vision*, pages 523–540. Springer, 2020. [2](#)
- [65] Alec Radford. Improving language understanding by generative pre-training, 2018. [1](#)
- [66] Alec Radford, Jeffrey Wu, Rewon Child, David Luan, Dario Amodei, Ilya Sutskever, et al. Language models are unsupervised multitask learners. *OpenAI blog*, 1(8):9, 2019. [1](#), [2](#), [5](#), [15](#)
- [67] Aditya Ramesh, Mikhail Pavlov, Gabriel Goh, Scott Gray, Chelsea Voss, Alec Radford, Mark Chen, and Ilya Sutskever. Zero-shot text-to-image generation. In *International conference on machine learning*, pages 8821–8831. Pmlr, 2021. [2](#)
- [68] Ali Razavi, Aaron Van den Oord, and Oriol Vinyals. Generating diverse high-fidelity images with vq-vae-2. *Advances in neural information processing systems*, 32, 2019. [3](#)
- [69] Ali Razavi, Aaron Van den Oord, and Oriol Vinyals. Generating diverse high-fidelity images with vq-vae-2. *Advances in neural information processing systems*, 32, 2019. [2](#), [5](#), [8](#)
- [70] Pradyumna Reddy, Ismail Elezi, and Jiankang Deng. G3dr: Generative 3d reconstruction in imagenet. In *Proceedings of the IEEE/CVF Conference on Computer Vision and Pattern Recognition*, pages 9655–9665, 2024. [2](#), [3](#)
- [71] Aditya Sanghi, Aliasghar Khani, Pradyumna Reddy, Arianna Rampini, Derek Cheung, Kamal Rahimi Malekshan, Kanika Madan, and Hooman Shayani. Wavelet latent diffusion (wala): Billion-parameter 3d generative model with compact wavelet encodings, 2024. [4](#), [16](#)
- [72] J Ryan Shue, Eric Ryan Chan, Ryan Po, Zachary Ankner, Jiajun Wu, and Gordon Wetzstein. 3d neural field generation using triplane diffusion. In *Proceedings of the IEEE/CVF Conference on Computer Vision and Pattern Recognition*, pages 20875–20886, 2023. [2](#), [3](#)
- [73] Vincent Sitzmann, Julien Martel, Alexander Bergman, David Lindell, and Gordon Wetzstein. Implicit neural representations with periodic activation functions. *Advances in Neural Information Processing Systems*, 33:7462–7473, 2020. [2](#)
- [74] Edward J Smith and David Meger. Improved adversarial systems for 3d object generation and reconstruction. In *Conference on Robot Learning*, pages 87–96. PMLR, 2017. [3](#)
- [75] Yongbin Sun, Yue Wang, Ziwei Liu, Joshua Siegel, and Sanjay Sarma. Pointgrow: Autoregressively learned point cloud generation with self-attention. In *Proceedings of the IEEE/CVF Winter Conference on Applications of Computer Vision*, pages 61–70, 2020. [2](#), [3](#)
- [76] Yu Sun, Shuohuan Wang, Shikun Feng, Siyu Ding, Chao Pang, Junyuan Shang, Jiaxiang Liu, Xuyi Chen, Yanbin

- Zhao, Yuxiang Lu, et al. Ernie 3.0: Large-scale knowledge enhanced pre-training for language understanding and generation. *arXiv preprint arXiv:2107.02137*, 2021. 1
- [77] Gemini Team, Rohan Anil, Sebastian Borgeaud, Jean-Baptiste Alayrac, Jiahui Yu, Radu Soricut, Johan Schalkwyk, Andrew M Dai, Anja Hauth, Katie Millican, et al. Gemini: a family of highly capable multimodal models. *arXiv preprint arXiv:2312.11805*, 2023. 1
- [78] Keyu Tian, Yi Jiang, Zehuan Yuan, Bingyue Peng, and Liwei Wang. Visual autoregressive modeling: Scalable image generation via next-scale prediction. *arXiv preprint arXiv:2404.02905*, 2024. 2, 3, 4, 14, 15, 16
- [79] Hugo Touvron, Thibaut Lavril, Gautier Izacard, Xavier Martinet, Marie-Anne Lachaux, Timothée Lacroix, Baptiste Rozière, Naman Goyal, Eric Hambro, Faisal Azhar, et al. Llama: Open and efficient foundation language models. *arXiv preprint arXiv:2302.13971*, 2023. 1
- [80] Hugo Touvron, Louis Martin, Kevin Stone, Peter Albert, Amjad Almahairi, Yasmine Babaei, Nikolay Bashlykov, Soumya Batra, Prajwal Bhargava, Shruti Bhosale, et al. Llama 2: Open foundation and fine-tuned chat models. *arXiv preprint arXiv:2307.09288*, 2023. 1
- [81] Aaron Van den Oord, Nal Kalchbrenner, Lasse Espeholt, Oriol Vinyals, Alex Graves, et al. Conditional image generation with pixelcnn decoders. *Advances in neural information processing systems*, 29, 2016. 3
- [82] Li Wang, Jie Yang, Weikai Chen, Xiaoxu Meng, Bo Yang, Jintao Li, and Lin Gao. Hsdf: Hybrid sign and distance field for modeling surfaces with arbitrary topologies. In *Advances in Neural Information Processing Systems*, 2022. 2
- [83] Xin Wen, Junsheng Zhou, Yu-Shen Liu, Hua Su, Zhen Dong, and Zhizhong Han. 3D shape reconstruction from 2D images with disentangled attribute flow. In *Proceedings of the IEEE/CVF Conference on Computer Vision and Pattern Recognition*, pages 3803–3813, 2022. 2
- [84] Xin Wen, Peng Xiang, Zhizhong Han, Yan-Pei Cao, Pengfei Wan, Wen Zheng, and Yu-Shen Liu. PMP-Net++: Point cloud completion by transformer-enhanced multi-step point moving paths. *IEEE Transactions on Pattern Analysis and Machine Intelligence*, 45(1):852–867, 2023. 2
- [85] Jiajun Wu, Chengkai Zhang, Tianfan Xue, Bill Freeman, and Josh Tenenbaum. Learning a probabilistic latent space of object shapes via 3d generative-adversarial modeling. *Advances in neural information processing systems*, 29, 2016. 3
- [86] Peng Xiang, Xin Wen, Yu-Shen Liu, Yan-Pei Cao, Pengfei Wan, Wen Zheng, and Zhizhong Han. Snowflake point deconvolution for point cloud completion and generation with skip-transformer. *IEEE Transactions on Pattern Analysis and Machine Intelligence*, 45(5):6320–6338, 2023. 2
- [87] Xingguang Yan, Liqiang Lin, Niloy J Mitra, Dani Lischinski, Daniel Cohen-Or, and Hui Huang. Shapeformer: Transformer-based shape completion via sparse representation. In *Proceedings of the IEEE/CVF Conference on Computer Vision and Pattern Recognition*, pages 6239–6249, 2022. 2, 3
- [88] Guandao Yang, Xun Huang, Zekun Hao, Ming-Yu Liu, Serge Belongie, and Bharath Hariharan. Pointflow: 3d point cloud generation with continuous normalizing flows. In *Proceedings of the IEEE/CVF international conference on computer vision*, pages 4541–4550, 2019. 3
- [89] Jianglong Ye, Yuntao Chen, Naiyan Wang, and Xiaolong Wang. GIFS: Neural implicit function for general shape representation. *Proceedings of the IEEE/CVF Conference on Computer Vision and Pattern Recognition*, 2022. 2
- [90] Jiahui Yu, Xin Li, Jing Yu Koh, Han Zhang, Ruoming Pang, James Qin, Alexander Ku, Yuanzhong Xu, Jason Baldridge, and Yonghui Wu. Vector-quantized image modeling with improved vqgan. *arXiv preprint arXiv:2110.04627*, 2021. 2
- [91] Jiahui Yu, Xin Li, Jing Yu Koh, Han Zhang, Ruoming Pang, James Qin, Alexander Ku, Yuanzhong Xu, Jason Baldridge, and Yonghui Wu. Vector-quantized image modeling with improved vqgan. *arXiv preprint arXiv:2110.04627*, 2021. 2
- [92] Lijun Yu, Jose Lezama, Nitesh Bharadwaj Gundavarapu, Luca Versari, Kihyuk Sohn, David Minnen, Yong Cheng, Agrim Gupta, Xiuye Gu, Alexander G Hauptmann, Boqing Gong, Ming-Hsuan Yang, Irfan Essa, David A Ross, and Lu Jiang. Language model beats diffusion - tokenizer is key to visual generation. In *The Twelfth International Conference on Learning Representations*, 2024. 8
- [93] Qihang Yu, Ju He, Xueqing Deng, Xiaohui Shen, and Liang-Chieh Chen. Randomized autoregressive visual generation. *arXiv preprint arXiv:2411.00776*, 2024. 2
- [94] Biao Zhang, Jiapeng Tang, Matthias Niessner, and Peter Wonka. 3dshape2vecset: A 3d shape representation for neural fields and generative diffusion models. *arXiv preprint arXiv:2301.11445*, 2023. 3
- [95] Wenyuan Zhang, Ruofan Xing, Yunfan Zeng, Yu-Shen Liu, Kanle Shi, and Zhizhong Han. Fast learning radiance fields by shooting much fewer rays. *IEEE Transactions on Image Processing*, 2023. 2
- [96] Xin-Yang Zheng, Hao Pan, Peng-Shuai Wang, Xin Tong, Yang Liu, and Heung-Yeung Shum. Locally attentional sdf diffusion for controllable 3d shape generation. *arXiv preprint arXiv:2305.04461*, 2023. 6, 7
- [97] Junsheng Zhou, Baorui Ma, Yu-Shen Liu, Yi Fang, and Zhizhong Han. Learning consistency-aware unsigned distance functions progressively from raw point clouds. In *Advances in Neural Information Processing Systems (NeurIPS)*, 2022. 2
- [98] Junsheng Zhou, Xin Wen, Yu-Shen Liu, Yi Fang, and Zhizhong Han. Self-supervised point cloud representation learning with occlusion auto-encoder. *arXiv e-prints*, pages arXiv–2203, 2022. 2
- [99] Junsheng Zhou, Baorui Ma, Shujuan Li, Yu-Shen Liu, and Zhizhong Han. Learning a more continuous zero level set in unsigned distance fields through level set projection. In *Proceedings of the IEEE/CVF international conference on computer vision*, 2023. 2, 3
- [100] Junsheng Zhou, Baorui Ma, Wenyuan Zhang, Yi Fang, Yu-Shen Liu, and Zhizhong Han. Differentiable registration

- of images and lidar point clouds with voxelpoint-to-pixel matching. In *Advances in Neural Information Processing Systems (NeurIPS)*, 2023. [2](#)
- [101] Junsheng Zhou, Jinsheng Wang, Baorui Ma, Yu-Shen Liu, Tiejun Huang, and Xinlong Wang. Uni3d: Exploring unified 3d representation at scale. *International Conference on Learning Representations*, 2024.
- [102] Junsheng Zhou, Xin Wen, Baorui Ma, Yu-Shen Liu, Yue Gao, Yi Fang, and Zhizhong Han. 3d-oae: Occlusion auto-encoders for self-supervised learning on point clouds. *IEEE International Conference on Robotics and Automation (ICRA)*, 2024. [2](#)
- [103] Junsheng Zhou, Weiqi Zhang, Baorui Ma, Kanle Shi, Yu-Shen Liu, and Zhizhong Han. Udiff: Generating conditional unsigned distance fields with optimal wavelet diffusion. In *Proceedings of the IEEE/CVF Conference on Computer Vision and Pattern Recognition*, pages 21496–21506, 2024. [1](#), [4](#), [6](#), [7](#), [16](#)
- [104] Heming Zhu, Yu Cao, Hang Jin, Weikai Chen, Dong Du, Zhangye Wang, Shuguang Cui, and Xiaoguang Han. Deep fashion3d: A dataset and benchmark for 3d garment reconstruction from single images. In *Computer Vision—ECCV 2020: 16th European Conference, Glasgow, UK, August 23–28, 2020, Proceedings, Part I 16*, pages 512–530. Springer, 2020. [4](#), [6](#), [7](#), [17](#)

3D-WAG: Hierarchical Wavelet-Guided Autoregressive Generation for High-Fidelity 3D Shapes

Supplementary Material

The supplementary material provides additional experimental details and evaluations of our approach, **3D-WAG**. The sections are organized as follows:

1. **Architectural Details:** Section 6 describes the architectural details of our approach.
2. **Implementation Details:** Section 7 provides additional implementation details and the hyper-parameters of our approach.
3. **Wavelet Inversion for 3D Mesh Extraction:** Section 8 discusses the extraction of 3D meshes from compact wavelet representations.
4. **Time Complexity Analysis:** Section 9 presents insights into the time-complexity analysis of our approach.
5. **Additional Results:** Section 10 showcases more results demonstrating the performance of our approach.
6. **Failure Cases:** Section 11 highlights the failure cases observed in our approach.

6. Architectural Details

The architecture of 3D-WAG draws inspiration from VAR [78], which has demonstrated superior performance compared to diffusion models in 2D image generation. In this work, we adapt the VAR framework to generate 3D shapes by modeling auto-regression as a coarse-to-fine detail prediction process. This is achieved by leveraging spatial frequency features extracted from the wavelet-based compact data representation of 3D shapes. To accommodate the 3D setting and wavelet-based input representation, the 3D-WAG architecture is extended and modified accordingly. Detailed information about the 3D-WAG architecture is provided below.

Stage 1: Autoencoder

The first stage of 3D-WAG involves training a U-Net based autoencoder similar to VQGAN framework [17]. We extend the U-Net architecture to process 3D data by replacing its 2D CNN layers with 3D CNNs, enabling efficient handling of volumetric wavelet features. To reconstruct or learn the wavelet-transformed inputs, which provide richer channel information at a lower volumetric spatial resolution, we modify the compression ratio of the architecture and adjust the dimensionality of the latent compact features. This adaptation yields a continuous latent representation with a channel dimensionality of 512 with a spatial resolution of 11^3 , optimized to capture both low and high-frequency components of 3D wavelet data effectively.

The Encoder and Decoder of 3D-WAG utilize 3D convolutional blocks, as detailed in Tables 6 and 7. The number of downsampling or compression levels, L , in the encoder and decoder stages is set to either 2 or 3, depending on the dataset size. For datasets with fewer samples, compression is reduced to better preserve distinguishing features between samples. Here, C_{in} and C_{out} represent the input and output channel dimensions, respectively, while H , W , and D denote the height, width, and depth of the wavelet data. C_z , corresponds to the channel dimension of the compact global feature map z .

Table 6. Encoder Architecture: Processes input features using 3D convolutions, residual blocks, and optional attention mechanisms, followed by downsampling to obtain a compact latent representation.

Encoder Stage	Operation	Output Dimensions
Input	-	$\mathbb{R}^{B \times C_{in} \times H \times W \times D}$
Initial Convolution	$\text{Conv3D}(C_{in}, C, 3, 1, 1)$	$\mathbb{R}^{B \times C \times H \times W \times D}$
Downsampling	For $i = 1, \dots, L$:	
Residual Block	$\text{ResNetBlock}(C_{in}, C_{out})$	$\mathbb{R}^{B \times C_{out} \times H \times W \times D}$
Attention Block	$\text{AttnBlock}(C_{out})$	Same as above
Downsample	Downsample2x	$\mathbb{R}^{B \times C_{out} \times \frac{H}{2} \times \frac{W}{2} \times \frac{D}{2}}$
Middle Layers	-	
Residual Block	$\text{ResNetBlock}(C, C)$	$\mathbb{R}^{B \times C \times \frac{H}{2^{L-1}} \times \frac{W}{2^{L-1}} \times \frac{D}{2^{L-1}}}$
Attention Block	$\text{AttnBlock}(C)$	Same as above
Residual Block	$\text{ResNetBlock}(C, C)$	Same as above
Output Convolution	$\text{Conv3D}(C, C_z, 3, 1, 1)$	$\mathbb{R}^{B \times C_z \times \frac{H}{2^{L-1}} \times \frac{W}{2^{L-1}} \times \frac{D}{2^{L-1}}}$
Output	-	Same as above

Table 7. Decoder Architecture: Reverses the encoder operations by progressively upsampling latent features to reconstruct the input dimensions.

Decoder Stage	Operation	Output Dimensions
Input	-	$\mathbb{R}^{B \times C_z \times \frac{H}{2^{L-1}} \times \frac{W}{2^{L-1}} \times \frac{D}{2^{L-1}}}$
Initial Convolution	$\text{Conv3D}(C_z, C, 3, 1, 1)$	$\mathbb{R}^{B \times C \times \frac{H}{2^{L-1}} \times \frac{W}{2^{L-1}} \times \frac{D}{2^{L-1}}}$
Middle Layers	-	
Residual Block	$\text{ResNetBlock}(C, C)$	Same as above
Attention Block	$\text{AttnBlock}(C)$	Same as above
Residual Block	$\text{ResNetBlock}(C, C)$	Same as above
Upsampling	For $i = L, \dots, 1$:	
Residual Block	$\text{ResNetBlock}(C_{in}, C_{out})$	$\mathbb{R}^{B \times C_{out} \times \frac{H}{2^{L-1}} \times \frac{W}{2^{L-1}} \times \frac{D}{2^{L-1}}}$
Attention Block	$\text{AttnBlock}(C_{out})$	Same as above
Upsample	Upsample2x	$\mathbb{R}^{B \times C_{out} \times 2H \times 2W \times 2D}$
Output Convolution	$\text{Conv3D}(C, C_{out}, 3, 1, 1)$	$\mathbb{R}^{B \times C_{out} \times H \times W \times D}$
Output	-	Same as above

Multi-Scale Quantization: In our approach, we adopt a multi-scale quantization scheme similar to the one proposed in [78] for 2D data, instead of directly quantizing the global latent feature map z into tokens. Specifically, the continuous global feature map z is quantized into K multi-scale

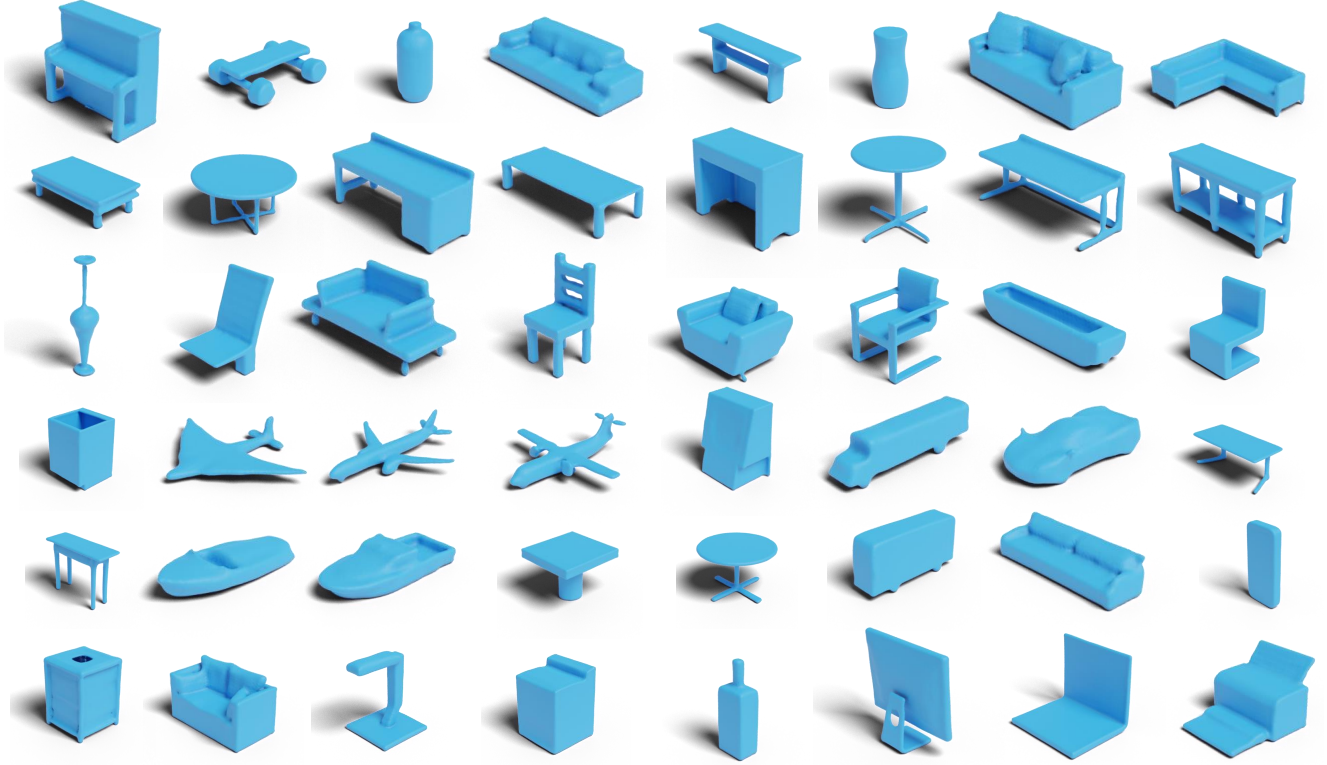


Figure 7. Examples of unconditional generation examples under the ShapeNet [7] dataset.

discrete token maps, denoted as $\{f_1, f_2, \dots, f_K\}$, where the highest resolution is represented by f_K . Each token map f_k has a resolution of (H_k, W_k, D_k) . To ensure consistency across scales, a shared codebook Z is utilized for quantization, such that the tokens at each scale f_k belong to the same vocabulary defined by Z . To address potential information loss when upsampling the lower-resolution latent feature maps f_k to the highest resolution (H_k, W_k, D_k) , we introduce $K - 1$ additional convolution layers, $\{C_j\}_{j=1}^{K-1}$. These layers refine the upscaled features to recover detailed information. These multi-scale token maps are important in modeling the generation of shapes. Higher-resolution token maps can be predicted from lower-resolution ones, facilitating a coarse-to-fine generation process.

Stage 2: Prior Model

We employ the GPT-2 decoder-only transformer model [66] to model auto-regressive shape generation, leveraging its demonstrated ability to generate high-resolution token maps from low-resolution token maps in image generation [78]. In this work, we adopt the same architecture to produce fine details from high resolution token maps starting from coarser, lower resolution token maps. To achieve this, we first flatten the multi-scale token maps, $\{f_1, f_2, \dots, f_K\}$, at each scale. Specifically, these token maps, originally de-

fined with dimensions (B, C_z, H_k, W_k, D_k) , where $k \in \{1, 2, 3, \dots, K\}$, are transformed into a sequence of token maps with dimensions (B, C_z, S_k) , where $S_k = H_k \times W_k \times D_k$ represents the spatial size of the token map at scale k , B is batch size and C_z represents the channel dimensionality of the token map. The decoder-only transformer network is then utilized to predict the token map at a higher scale based on the token map at a lower scale. This auto-regressive generation process is performed iteratively over the token maps $\{f_k\}$, progressively enabling the model to generate shapes from coarse to fine resolution details.

7. Implementation Details

We outline the implementation details and hyperparameters used in our approach. The training was conducted on two types of GPUs: 4 NVIDIA H100 GPUs with 93.58 GB of VRAM each and 4 NVIDIA A40 GPUs with 44.98 GB of VRAM each. In the first stage, during training, we used 11 scales of quantization, which means 11 token maps are learned to model the second stage of 3D-WAG generation process. The codebook size (Z) was set to 8192 for the DeepFashion3D and ShapeNet subset datasets, while for the full ShapeNet dataset, it was increased to $Z = 16384$. The model was trained with a learning rate of 1×10^{-4} and a batch size of 48 on 4 GPUs parallel.

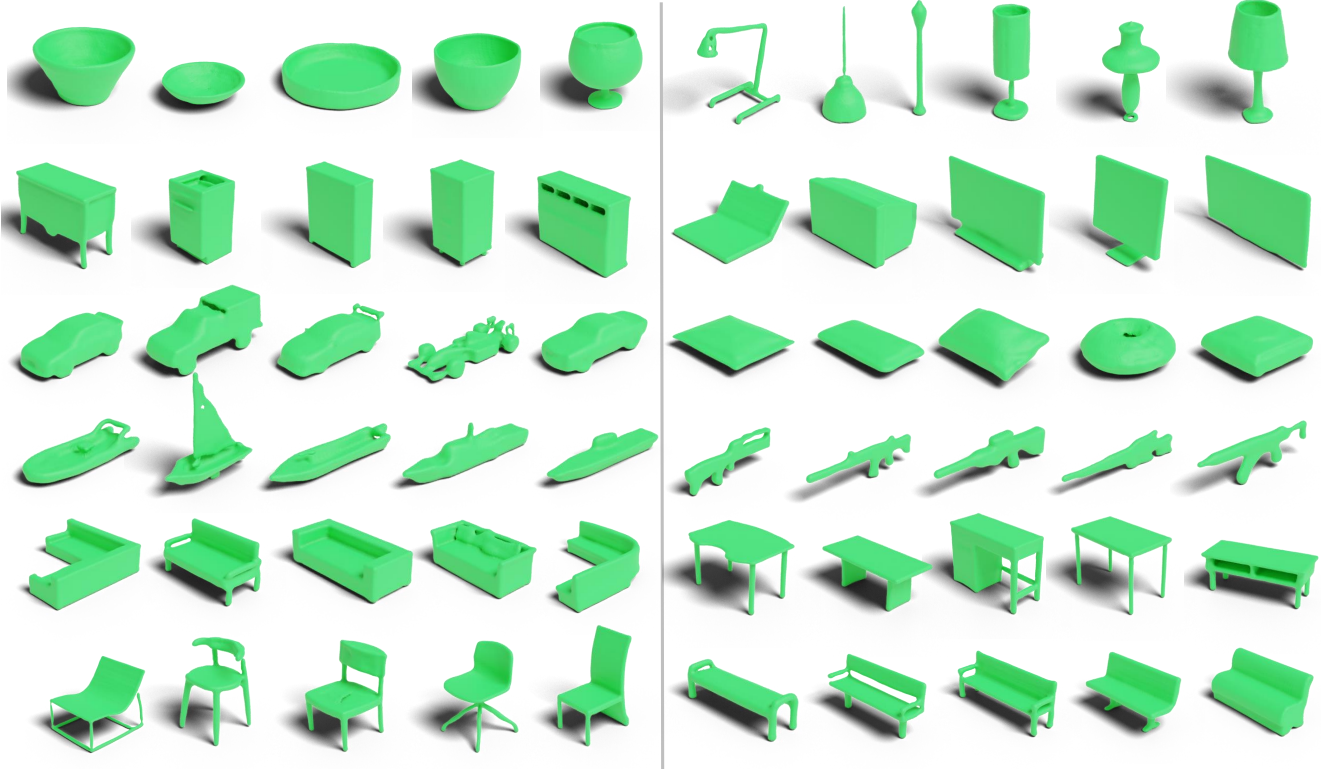


Figure 8. Class-conditional generation results on the ShapeNet [7] dataset. Twelve categories are illustrated, with two categories per row. Categories from left to right, top to bottom, are: Bowl, Lamp; Cabinet, Monitor; Car, Pillow; Watercraft, Rifle; Sofa, Table; Chair, Bench. Each category showcases the diversity of shapes generated within its class.

For the Signed Distance Fields (SDF), we used a wavelet-based input representation with dimensions $(1, 64, 46, 46, 46)$, following the design in [71]. For the Unsigned Distance Fields (UDF), we adopted the representation proposed in [103], where the low frequency wavelet components are represented at a resolution of 46^3 , and the high frequency wavelet components are represented at a resolution of 76^3 . These components are fused using a learnable layer, resulting in a compact wavelet representation with a resolution of 46^3 . This fusion retains high-frequency information while ensuring compatibility with our approach which expects 46^3 spatial resolution. For stage-2 prior model training, we use same hyperparameter setting as in VAR [78] with embedding dimension of 8192.

8. Wavelet Inversion

As discussed in the main paper, we employ the compact wavelet-based input representation from recent works [71, 103] to represent Signed Distance Fields (SDF) and the Unsigned Distance Fields (UDF) respectively. We utilize the same implicit function extraction techniques outlined in [71] and [103] for generating the respective implicit representations from compact wavelet data. Later, we use

marching cubes in case extracting the surfaces from SDF and DCUDF [22] to extract the surface from UDF, ensuring a fair comparison with prior works.

9. Time Complexity of 3D-WAG Generation

In this section, we compare the time complexity of a standard autoregressive (AR) model with that of our proposed 3D-WAG approach. While AR models incur high computational costs due to their quadratic scaling in self-attention, 3D-WAG reduces complexity by employing a progressive resolution strategy. Below, we derive the time complexities of both methods. We refer to [78] for the image analog of this derivation.

AR generation complexity For a standard AR model, implemented with a self-attention transformer, the time complexity is $\mathcal{O}(n^9)$ for generating a volume of size $x \times y \times z = n^3$ (assuming $x = y = z = n$).

Proof: At each iteration $1 \leq i \leq n^3$, the model performs $\mathcal{O}(i^2)$ computations due to the quadratic scaling of self-attention with the number of tokens. The total time complexity is therefore:

$$\sum_{i=1}^{n^3} i^2 = \frac{n^3(n^3+1)(2n^3+1)}{6} \sim n^9 \quad (3)$$

3D-WAG complexity. In contrast, 3D-WAG generates volumes autoregressively at progressively increasing resolutions. Specifically, the generated volumes have sizes $(x_1, y_1, z_1), (x_2, y_2, z_2), \dots, (x_k, y_k, z_k), \dots, (x_K, y_K, z_K)$, which we assume satisfy $x_k = y_k = z_k = n_k$. In our experiments, the resolution n_k grows sub-linearly with the step index k , and we parameterize this growth as $n_k = a^{k-1}$, where $a > 1$. This progressive resolution strategy significantly reduces the computational cost, achieving a time complexity of $\mathcal{O}(n^6)$, as shown below.

Proof: The total number of tokens up to step k is given by the geometric sum:

$$\sum_{i=1}^k n_i^3 = \sum_{i=1}^k a^{3(i-1)} = \frac{1 - a^{3k}}{1 - a^3} \quad (4)$$

The computational complexity of generating all tokens up to step k is proportional to the square of this quantity, since at each step the attention mechanism operates on all previously generated tokens. Thus:

$$\text{Time complexity} \sim \sum_{k=1}^K \left(\frac{1 - a^{3k}}{1 - a^3} \right)^2 \quad (5)$$

The dominant term in the geometric sum is a^{3k} , and so:

$$\sum_{k=1}^K \left(\frac{1 - a^{3k}}{1 - a^3} \right)^2 \sim \sum_{k=1}^K a^{6k} \sim a^{6K} \quad (6)$$

Using $K = \log_a(n) + 1$ (where n is the resolution of the final volume), it follows that the total time complexity is $\mathcal{O}(n^6)$.

10. Additional Results

In this section, we present additional results generated by 3D-WAG.

Unconditional Generation: Figure 7 showcases examples from the unconditional generation setting. The model was trained on the entire ShapeNet dataset, consisting of approximately 55000 samples. The results highlight the diversity of the generated shapes and their consistency with the characteristics of the training data.

Class-Conditional Generation: Additional examples of conditional generation are provided in Figure 8. For these results, the model was trained on a subset of ShapeNet containing 15 classes, using class labels as conditioning inputs. These results demonstrate the model’s ability to adaptively generate shapes based on the provided class labels.

Ablation Study on Codebook Size To analyze the impact of codebook size on the reconstruction performance of our proposed 3D-WAG approach, we conducted an ablation study. Specifically, we evaluated the reconstruction

error between the input wavelet volume data and the predicted wavelet data from the validation set of the ShapeNet dataset, which includes 55 categories.

Table 8 summarizes the results of reconstruction loss evaluated using mean square error loss between the input and predictions by our approach. The findings indicate that a larger codebook size is advantageous as it provides greater diversity by accommodating more shape information and therefore improves reconstruction performance.

Table 8. Reconstruction error for different codebook sizes.

Codebook Size	Reconstruction Error
8192	0.00005
16,384	0.00002

11. Failure Cases



Figure 9. Examples of failure cases produced by 3D-WAG. On the left, we show samples from the unconditional generation setting, where shapes exhibit lacking clear semantic meaning (first shape), incomplete details (missing legs of the chair), or artifacts (holes in the table). On the right, in the text-to-3D generation task, the produced shapes fail to fully capture the prompt information, as the dress has one sleeve.

Our model occasionally generates shapes with incomplete details or unclear semantic meaning in the generation setting. We show examples of this behavior in Figure 9 (left). In the text-to-3D generation scenario, the output may fail to fully represent the prompt’s specifications, as illustrated in Figure 9 (right). These limitations can be attributed to the relatively small size of the datasets. Specifically, the datasets used for text-to-3D generation were particularly limited, while ShapeNet [7] and DeepFashion3D [104], containing about 55000 and 1798 samples respectively, are not considered large-scale datasets. We hypothesize that scaling our approach to larger datasets could significantly reduce the frequency of such failure cases, consistent with findings in prior studies on similar tasks [30].